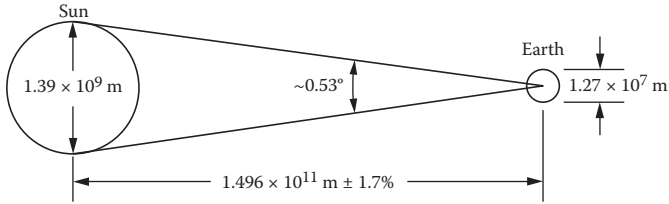

Figure 2.1
Relationship between the sun and the earth.

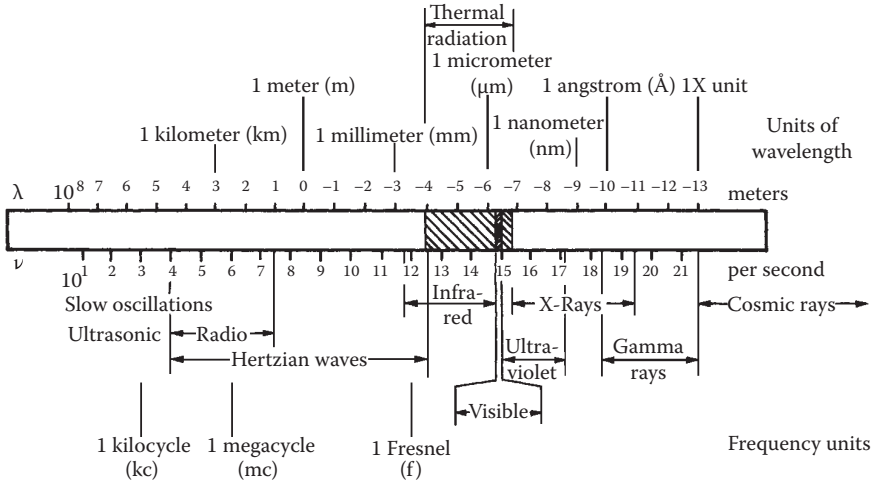

Figure 2.2
Electromagnetic radiation spectrum.

002x002.eps

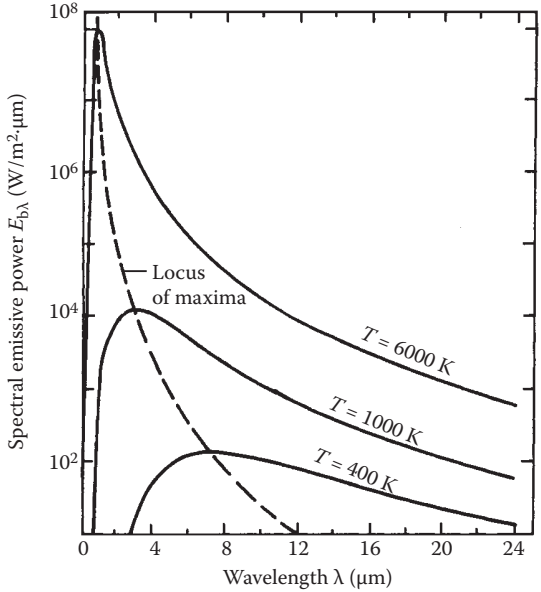

Figure 2.3
Spectral distribution of black-body radiation.

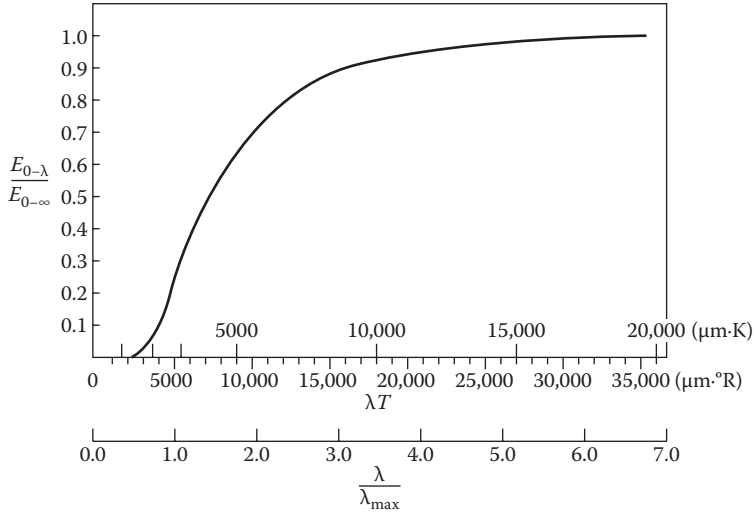

Figure 2.4
Fraction of total emissive power in spectral region between $\lambda = 0$ and λ as a function of λT and λ/λ_{max}.

λ/λ_{max}	$\frac{E_{b\lambda}}{E_{b\lambda,max}}$	$\frac{E_{b\lambda,0-\lambda}}{\sigma T^4}$	λ/λ_{max}	$\frac{E_{b\lambda}}{E_{b\lambda,max}}$	$\frac{E_{b\lambda,0-\lambda}}{\sigma T^4}$	λ/λ_{max}	$\frac{E_{b\lambda}}{E_{b\lambda,max}}$	$\frac{E_{b\lambda,0-\lambda}}{\sigma T^4}$
0.00	0.0000	0.0000	1.50	0.7103	0.5403	2.85	0.1607	0.8661
0.20	0.0000	0.0000	1.55	0.6737	0.5630	2.90	0.1528	0.8713
0.25	0.0003	0.0000	1.60	0.6382	0.5846	2.95	0.1454	0.8762
0.30	0.0038	0.0001	1.65	0.6039	0.6050	3.00	0.1384	0.8809
0.35	0.0187	0.0004	1.70	0.5710	0.6243	3.10	0.1255	0.8895
0.40	0.0565	0.0015	1.75	0.5397	0.6426	3.20	0.1141	0.8974
0.45	0.1246	0.0044	1.80	0.5098	0.6598	3.30	0.1038	0.9045
0.50	0.2217	0.0101	1.85	0.4815	0.6761	3.40	0.0947	0.9111
0.55	0.3396	0.0192	1.90	0.4546	0.6915	3.50	0.0865	0.9170
0.60	0.4664	0.0325	1.95	0.4293	0.7060	3.60	0.0792	0.9225
0.65	0.5909	0.0499	2.00	0.4054	0.7197	3.70	0.0726	0.9275
0.70	0.7042	0.0712	2.05	0.3828	0.7327	3.80	0.0667	0.9320
0.75	0.8007	0.0960	2.10	0.3616	0.7449	3.90	0.0613	0.9362
0.80	0.8776	0.1236	2.15	0.3416	0.7565	4.00	0.0565	0.9401
0.85	0.9345	0.1535	2.20	0.3229	0.7674	4.20	0.0482	0.9470
0.90	0.9725	0.1849	2.25	0.3053	0.7777	4.40	0.0413	0.9528
0.95	0.9936	0.2172	2.30	0.2887	0.7875	4.60	0.0356	0.9579
1.00	1.0000	0.2501	2.35	0.2731	0.7967	4.80	0.0308	0.9622
1.05	0.9944	0.2829	2.40	0.2585	0.8054	5.00	0.0268	0.9660
1.10	0.9791	0.3153	2.45	0.2447	0.8137	6.00	0.0142	0.9790
1.15	0.9562	0.3472	2.50	0.2318	0.8215	7.00	0.0082	0.9861
1.20	0.9277	0.3782	2.55	0.2197	0.8290	8.00	0.0050	0.9904
1.25	0.8952	0.4081	2.60	0.2083	0.8360	9.00	0.0033	0.9930
1.30	0.8600	0.4370	2.65	0.1976	0.8427	10.00	0.0022	0.9948
1.35	0.8231	0.4647	2.70	0.1875	0.8490	20.00	0.0002	0.9993
1.40	0.7854	0.4911	2.75	0.1780	0.8550	40.00	0.0000	0.9999
1.45	0.7477	0.5163	2.80	0.1691	0.8607	50.00	0.0000	1.0000

λ = wavelength in micrometer.

λ_{max} = wavelength at $E_{b\lambda,max}$ in micrometer = $2898/T$.

$E_{b\lambda}$ = monochromatic emissive power in $W/m^2 \cdot \mu m$

$= 374.15 \times 10^6/\lambda^5 [\exp(14{,}387.9/\lambda T) - 1]$,

$E_{b\lambda,max}$ = maximum monochromatic emissive power in $W/m^2 \cdot \mu m$

$= 12.865 \times 10^{-12} T^5$,

$E_{b\lambda,0-\lambda} = \int_0^{\lambda} E_{b\lambda}\, d\lambda$,

$\sigma T^4 = E_{b\lambda,0-\infty} = 5.670 \times 10^{-8} T^4\ W/m^2$, and

T = absolute temperature in Kelvin.

Figure 2.5
Thermal radiation functions.

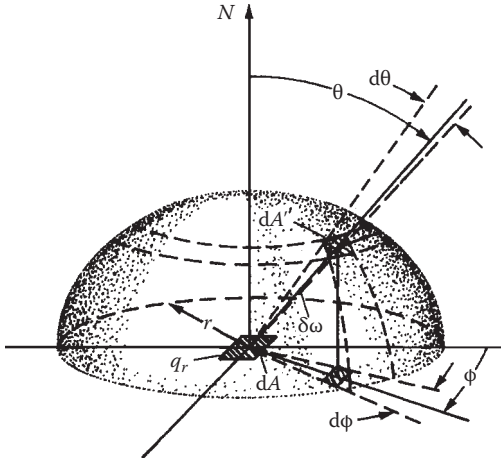

Figure 2.6
Schematic diagram illustrating radiation intensity and flux.

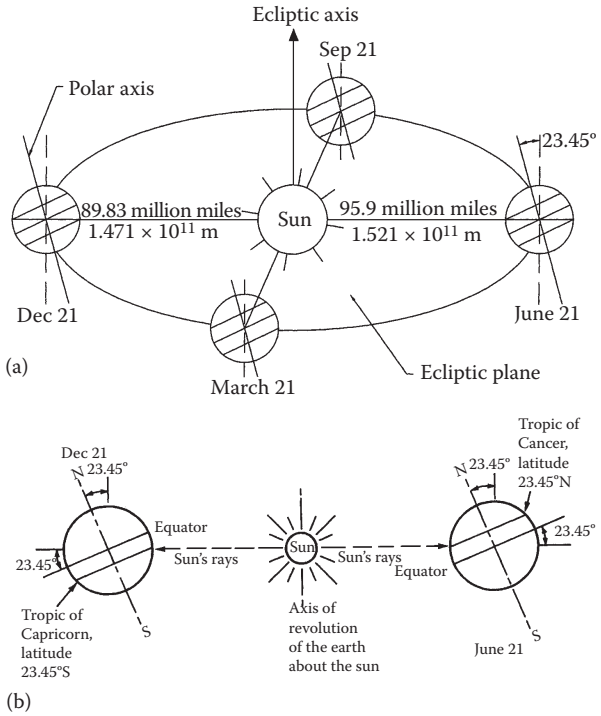

Figure 2.7
(a) Motion of the earth about the sun. (b) Location of tropics. Note that the sun is so far from the earth that all the rays of the sun may be considered as parallel to one another when they reach the earth.

		Declination		Equation of time				Declination		Equation of time	
Date		Deg	Min	Min	Sec	Date		Deg	Min	Min	Sec
Jan	1	−23	4	−3	14	Feb	1	−17	19	−13	34
	5	−22	42	−5	6		5	−16	10	−14	2
	9	−22	13	−6	50		9	−14	55	−14	17
	13	−21	37	−8	27		13	−13	37	−14	20
	17	−20	54	−9	54		17	−12	15	−14	10
	21	−20	5	−11	10		21	−10	50	−13	50
	25	−19	9	−12	14		25	−9	23	−13	19
	29	−18	9	−13	5						
Mar	1	−7	53	−12	38	Apr	1	+4	14	−4	12
	5	−6	21	−11	48		5	5	46	−3	1
	9	−5	48	−10	51		9	7	17	−1	52
	13	−3	14	−9	49		13	8	46	−0	47
	17	−1	39	−8	42		17	10	12	+0	13
	21	−0	5	−7	32		21	11	35	1	6
	25	+1	30	−6	20		25	12	56	1	53
	29	3	4	−5	7		29	14	13	2	33
May	1	+14	50	+2	50	Jun	1	+21	57	2	27
	5	16	2	3	17		5	22	28	1	49
	9	17	9	3	35		9	22	52	1	6
	13	18	11	3	44		13	23	10	+0	18
	17	19	9	3	44		17	23	22	−0	33
	21	20	2	3	24		21	23	27	−1	25
	25	20	49	3	16		25	23	25	−2	17
	29	21	30	2	51		29	23	17	−3	7
Jul	1	+23	10	−3	31	Aug	1	+18	14	−6	17
	5	22	52	−4	16		5	17	12	−5	59
	9	22	28	−4	56		9	16	6	−5	33
	13	21	57	−5	30		13	14	55	−4	57
	17	21	21	−5	57		17	13	41	−4	12
	21	20	38	−6	15		21	12	23	−3	19
	25	19	50	−6	24		25	11	2	−2	18
	29	18	57	−6	23		29	9	39	−1	10
Sep	1	+8	35	−0	15	Oct	1	−2	53	+10	1
	5	7	7	+1	2		5	−4	26	11	17
	9	5	37	2	22		9	−5	58	12	27
	13	4	6	3	45		13	−7	29	13	30
	17	2	34	5	10		17	−8	58	14	25
	21	1	1	6	35		21	−10	25	15	10
	25	0	32	8	0		25	−11	50	15	46
	29	−2	6	9	22		29	−13	12	16	10

Figure 2.8
Summary of solar ephemeris. Since each year is 365.25 days long, the precise value of declination varies from year to year. *The American Ephemeris and Nautical Almanac*, published each year by the US Government Printing Office, contains precise values for each day of each year.

(*Continued*)

		Declination		Equation of time				Declination		Equation of time	
Date		Deg	Min	Min	Sec	Date		Deg	Min	Min	Sec
Nov	1	−14	11	+16	21	Dec	1	−21	41	11	16
	5	−15	27	16	23		5	−22	16	9	43
	9	−16	38	16	12		9	−22	45	8	1
	13	−17	45	15	47		13	−23	6	6	12
	17	−18	48	15	10		17	−23	20	4	47
	21	−19	45	14	18		21	−23	26	2	19
	25	−20	36	13	15		25	−23	25	+0	20
	29	−21	21	11	59		29	−23	17	−1	39

Figure 2.8 (Continued)
Summary of solar ephemeris. Since each year is 365.25 days long, the precise value of declination varies from year to year. *The American Ephemeris and Nautical Almanac*, published each year by the US Government Printing Office, contains precise values for each day of each year.

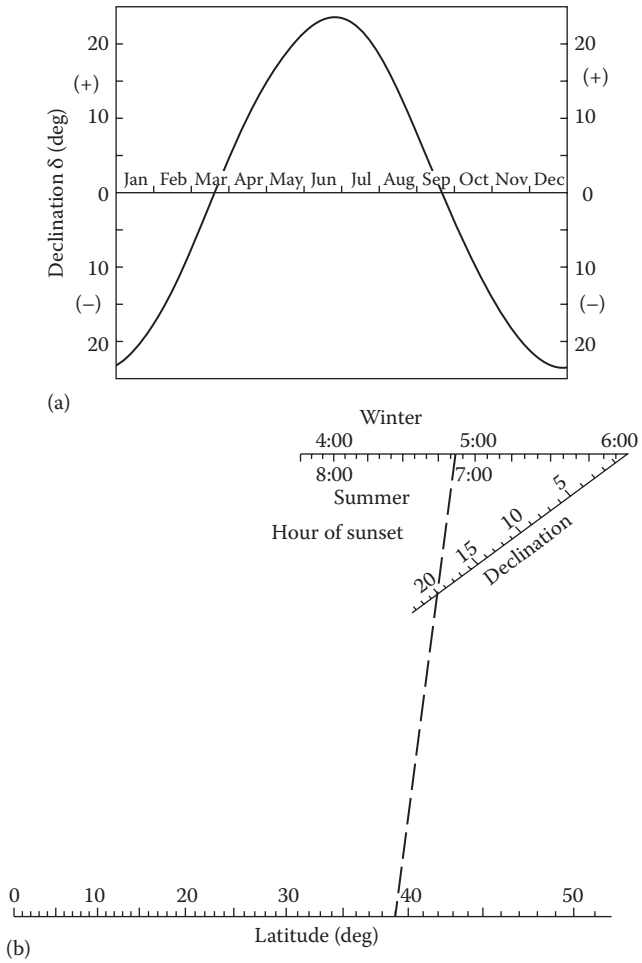

Figure 2.9
(a) Graph to determine the solar declination. (b) Sunset nomograph example. Example b shows determination of sunset time for summer (7:08 p.m.) and winter (4:52 p.m.) when the latitude is 39°N and the solar declination angle is 20°. (From Whillier, A., *Sol Energy* 9, 165–166, 1965.)

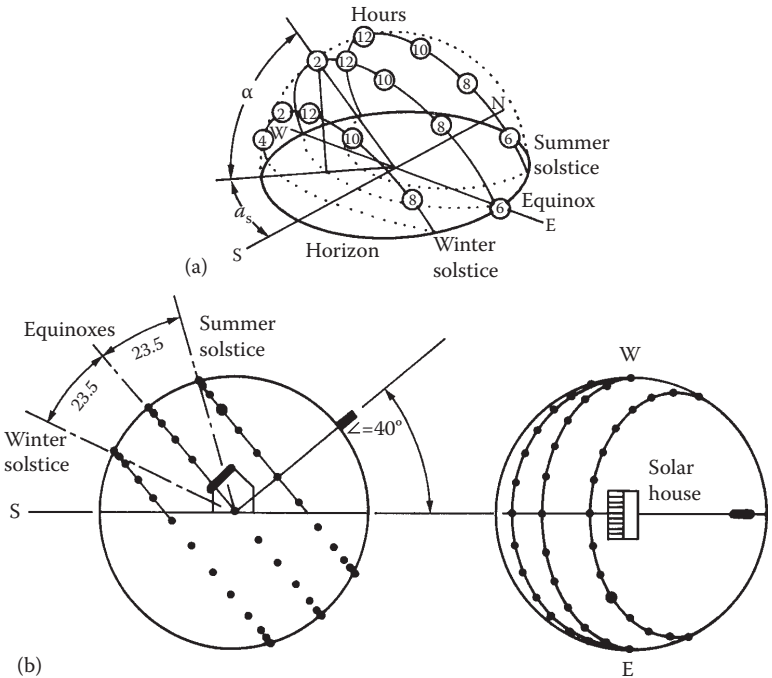

Figure 2.10
Sun paths for the summer solstice (6/21), the equinoxes (3/21 and 9/21), and the winter solstice (12/21) for a site at 40°N: (a) isometric view; (b) elevation and plan views.

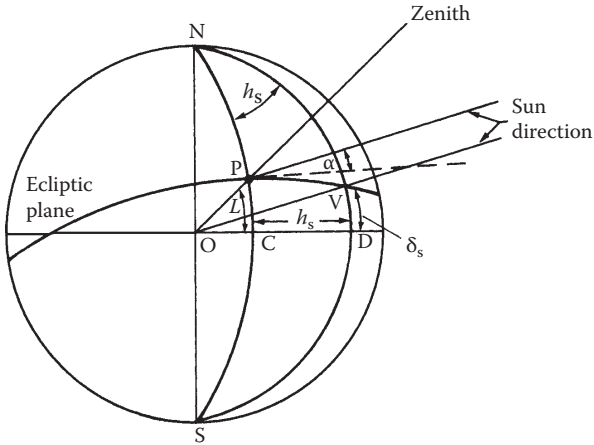

Figure 2.11
Definition of solar hour angle h_s (CND), solar declination δ_s (VOD), and latitude L (POC); P, site of interest. (Modified from Kreider, J.F. and F. Kreith, *Solar Heating and Cooling*, Washington, DC: Hemisphere Publ. Corp., 1982.)

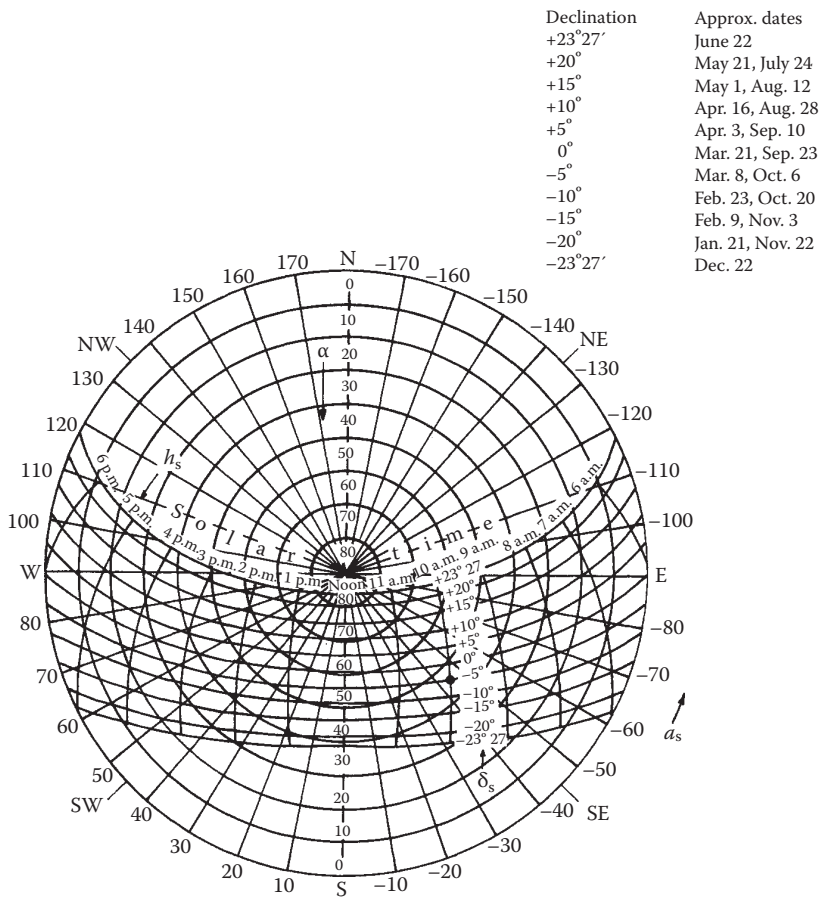

Figure 2.12
Sun-path diagram for 30°N latitude showing altitude and azimuth angles. (Modified from Kreider, J.F. and F. Kreith, *Solar Heating and Cooling*, revised 1st ed. Washington, DC: Hemisphere Publ. Corp., 1977.)

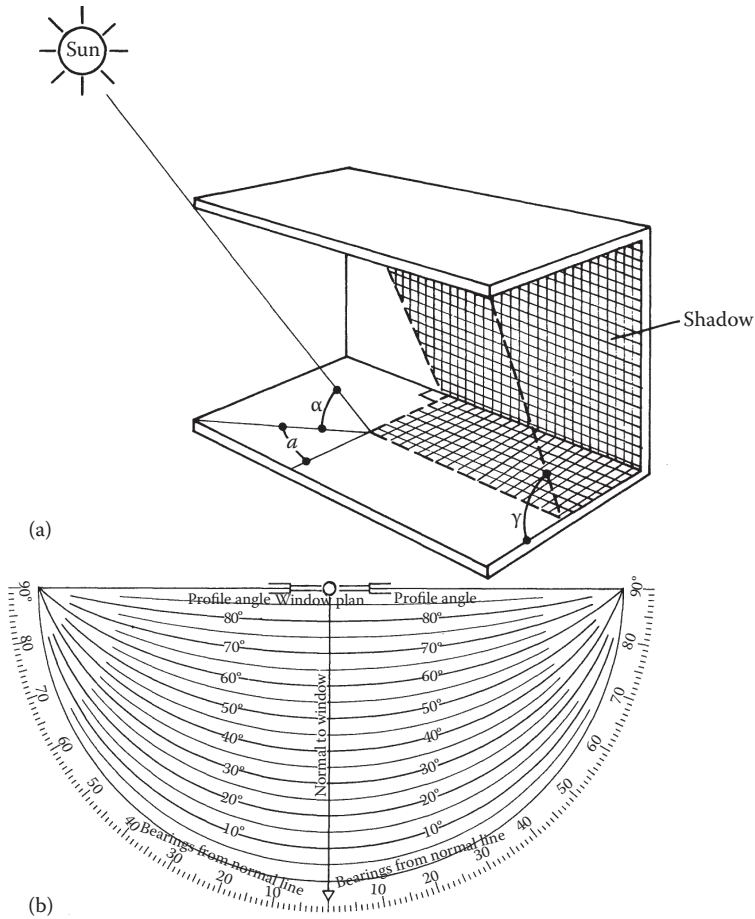

Figure 2.13
(a) Sketch showing the profile angle γ and the corresponding solar altitude angle α for a window shading device; (b) the shadow-angle protractor. (With permission from the Libby–Owens–Ford Glass Co.)

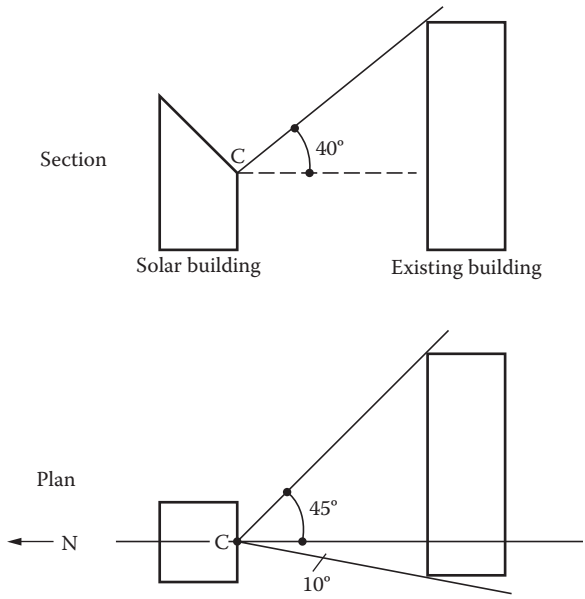

Figure 2.14
Plan and elevation view of proposed solar building and existing building, which may shade solar collector at point C.

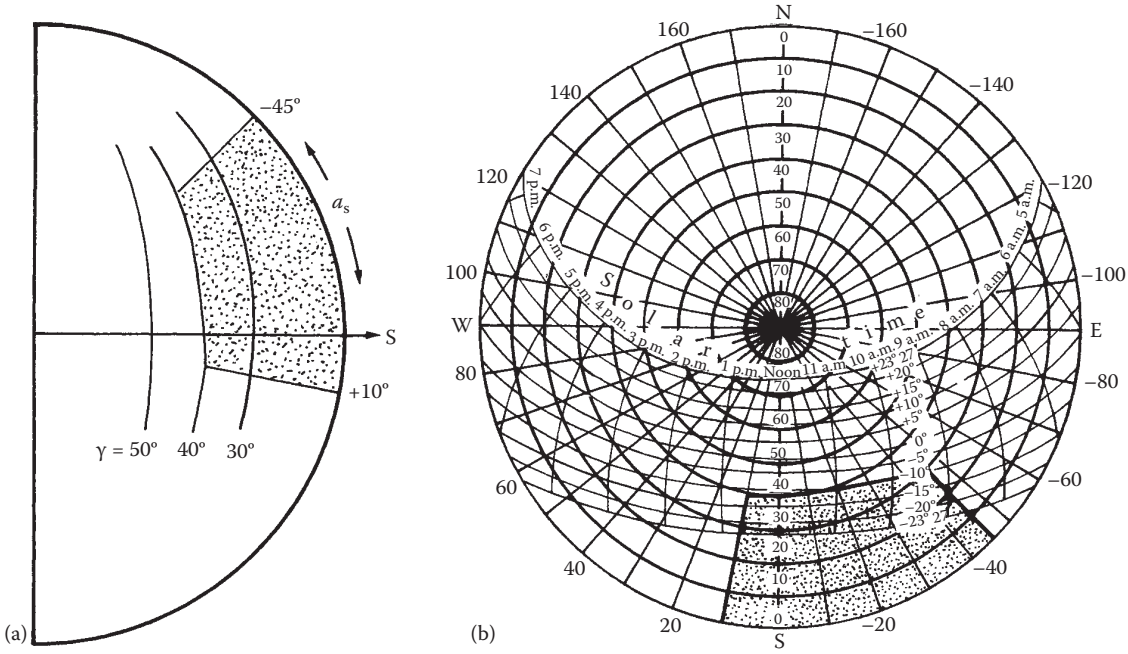

Figure 2.15
(a) Shadow map constructed for the example shown in Figure 2.14; (b) shadow map superimposed on a sun-path diagram.

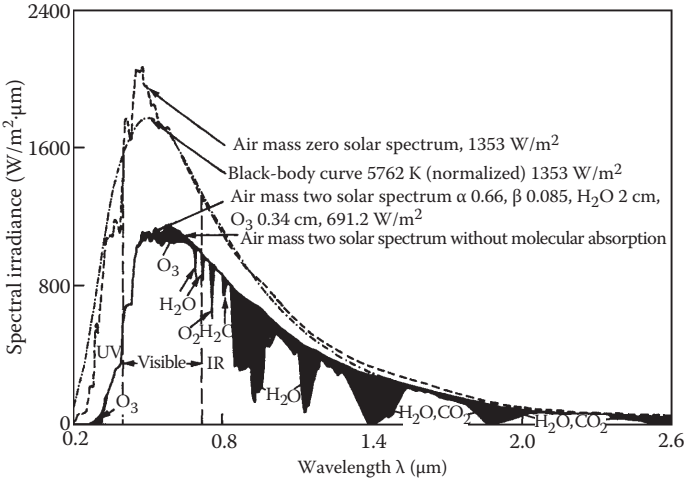

Figure 2.16
Extraterrestrial solar radiation spectral distribution. Also shown are equivalent black-body and atmosphere-attenuated spectra.

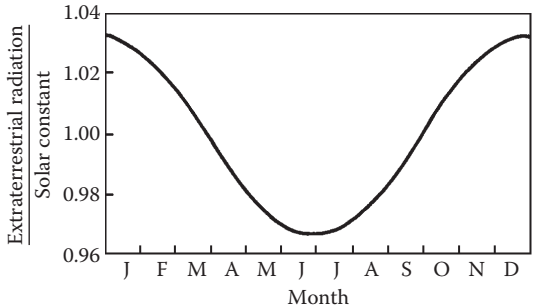

Figure 2.17
Effect of the time of year on the ratio of extraterrestrial radiation to the nominal solar constant.

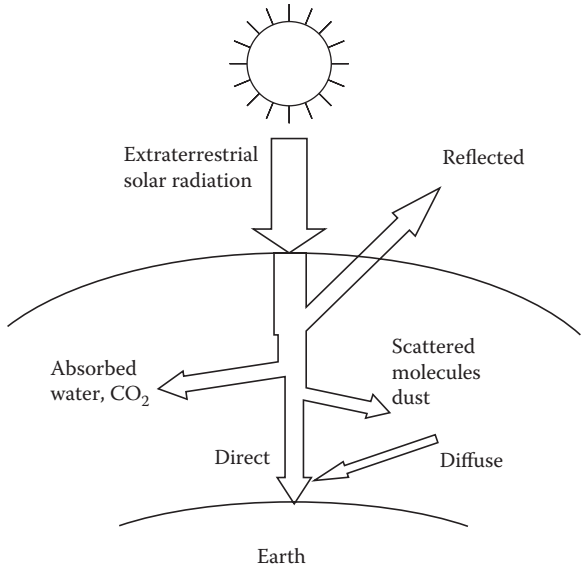

Figure 2.18
Attenuation of solar radiation as it passes through the atmosphere.

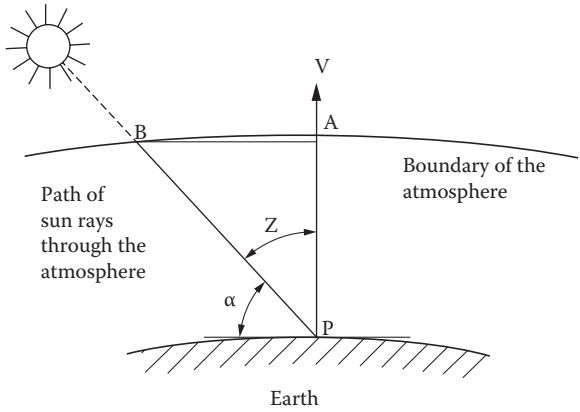

Figure 2.19
Air mass definition; air mass m = BP/AP = cosec α, where α is the altitude angle. The atmosphere is idealized as a constant thickness layer.

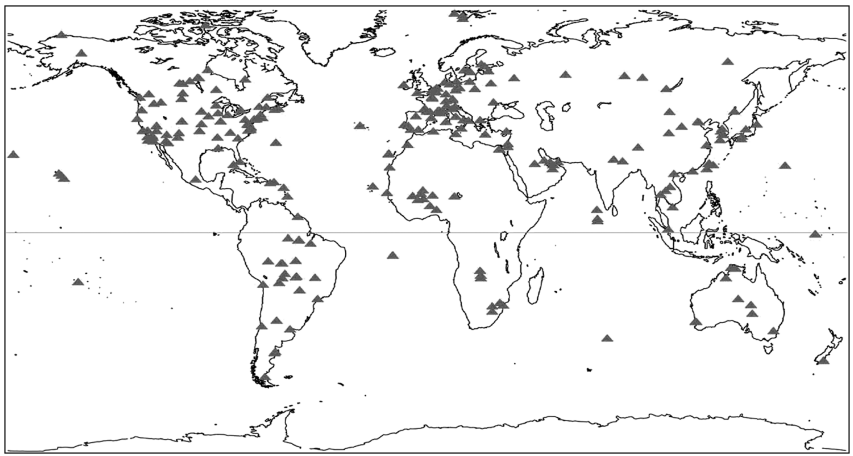

Figure 2.20
World sites of interest used in the model. (From Gueymard, C.A. and D. Thevenard, *Sol Energy* 83, 1998–2018, 2009.)

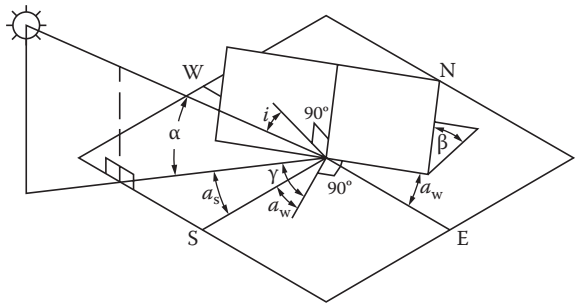

Solar altitude angle	α
Solar azimuth angle	a_s
Panel tilt angle	β
Panel azimuth angle	a_w
Incident angle	i

Figure 2.21
Definitions of solar angles for a tilted surface.

Authors	Measured data correlated	Correlation equations
Iqbal (1979)	Canada, 3 locations	$\frac{\bar{D}_h}{\bar{H}_h} = 0.791 - 0.635\left(\frac{\bar{n}}{\bar{N}}\right)$ $\frac{\bar{H}_d}{\bar{H}_h} = 0.163 + 0.478\left(\frac{\bar{n}}{\bar{N}}\right) - 0.655\left(\frac{\bar{n}}{\bar{N}}\right)^2$ $\frac{\bar{H}_b}{\bar{H}_{o,h}} = -0.176 + 1.45\left(\frac{\bar{n}}{\bar{N}}\right) - 1.12\left(\frac{\bar{n}}{\bar{N}}\right)^2$
Garg and Garg (1985)	India, 11 locations, 20 years' data	$\frac{\bar{H}_h}{\bar{H}_{o,h}} = 0.3156 + 0.4520\left(\frac{\bar{n}}{\bar{N}}\right)^2$ $\frac{\bar{D}_h}{\bar{H}_{o,h}} = 0.3616 - 0.2123\left(\frac{\bar{n}}{\bar{N}}\right)$ $\frac{\bar{D}_h}{\bar{H}_h} = 0.8677 - 0.7365\left(\frac{\bar{n}}{\bar{N}}\right)$
Hussain (1994)	India	$\frac{\bar{H}_h}{\bar{H}_{o,h}} = 0.394 + 0.364\left[\frac{\bar{n}}{\bar{N}'}\right] - 0.0035 W_{at}$ $\frac{\bar{D}_h}{\bar{H}_{o,h}} = 0.306 - 0.165\left[\frac{\bar{n}}{\bar{N}'}\right] - 0.0025 W_{at}$
Coppolino (1994)	Italy	$\frac{\bar{H}_h}{\bar{H}_{o,h}} = 0.67\left(\frac{\bar{n}}{\bar{N}}\right)^{0.45} \sin(\alpha_{sn})^{0.05}$ α_{sn} = Solar elevation at noon on the 15th of each month, degrees $0.15 \le \frac{\bar{n}}{\bar{N}} \le 0.90$
Akinoglu and Ecevit (1990)	Italy	$\frac{\bar{H}_h}{\bar{H}_{o,h}} = 0.145 + 0.845\left(\frac{\bar{n}}{\bar{N}}\right) - 0.280\left(\frac{\bar{n}}{\bar{N}}\right)^2$
Ögelman et al. (1984)	Turkey, 2 locations, 3 years' data	$\left(\frac{\bar{H}_h}{\bar{H}_{o,h}}\right) = 0.204 + 0.758\left(\frac{\bar{n}}{\bar{N}}\right) - 0.250\left\{\left[\left(\frac{\bar{n}}{\bar{N}}\right)^2\right]^2 + \sigma_{\frac{\bar{n}}{\bar{N}}}^2\right\}$ $\sigma_{\frac{\bar{n}}{\bar{N}}}^2 = 0.035 + 0.326\left(\frac{\bar{n}}{\bar{N}}\right) - 0.433\left(\frac{\bar{n}}{\bar{N}}\right)^2$
Gopinathan (1988)	40 locations around the world	$\frac{\bar{H}_h}{\bar{H}_{o,h}} = a + b\left(\frac{\bar{n}}{\bar{N}}\right)$ $a = -0.309 + 0.539\cos L - 0.0639h + 0.290\left(\frac{\bar{n}}{\bar{N}}\right)$ $b = 1.527 - 1.027\cos L + 0.0926h + 0.359\left(\frac{\bar{n}}{\bar{N}}\right)$

Figure 2.22
Angström–page-type correlations for specific locations. ($\bar{H}_a$, $\bar{H}_b$, $\bar{H}_{o,h}$, and $\bar{D}_h$ are monthly averaged daily values; $\bar{N}$ = maximum duration for which the Campbell–Stokes recorder can be active, that is, solar elevation >5°; W_{at} = relative humidity × (4.7923 + 0.3647T + 0.055T^2 + 0.0003T^3); T = ambient temperature (°C); W_{at} = g moisture/m³; h = elevation in kilometers above sea level; L = latitude.)

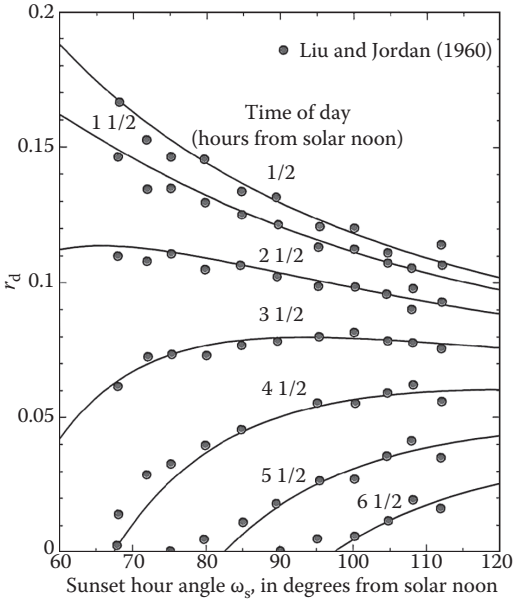

Figure 2.23
Collares-Pereira and Rabl Model, CPR. (Adapted from Collares-Pereira, M. and A. Rabl, *Sol Energy* 22, 155–166, 1979; Liu, B.H.Y. and R.C. Jordan, *Sol Energy* 4, 1–19, 1960. See also Liu, B.Y.H., Characteristics of solar radiation and the performance of flat plate solar energy collectors, PhD dissertation, University of Minnesota, Minneapolis, 1960.)

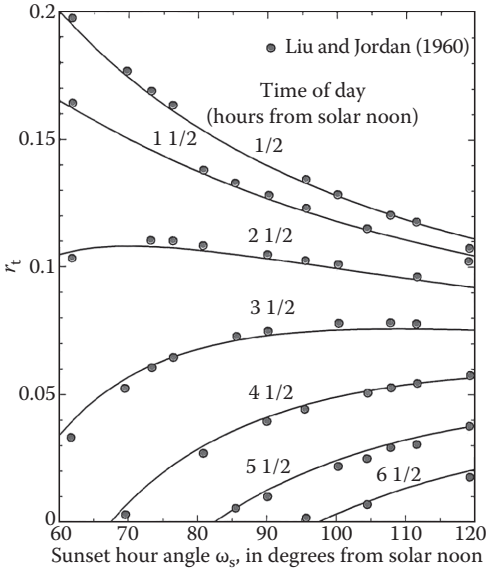

Figure 2.24
Collares-Pereira and Rabl Model modified by Gueymard (1986). (Adapted from Collares-Pereira, M. and A. Rabl, *Sol Energy* 22, 155–166, 1979; Liu, B.H.Y. and R.C. Jordan, *Sol Energy* 4, 1–19, 1960. See also Liu, B.Y.H., Characteristics of solar radiation and the performance of flat plate solar energy collectors, PhD dissertation, University of Minnesota, Minneapolis, 1960.)

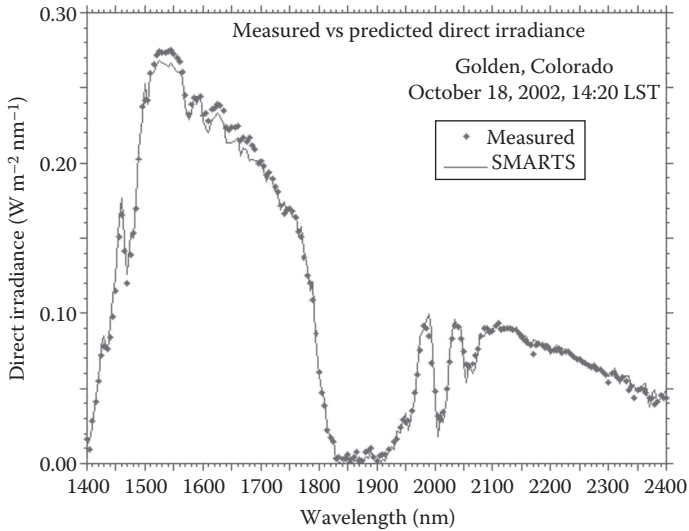

Figure 2.25
A sample spectral irradiance prediction compared with measured data for Golden, Colorado. (Taken from http://www.solarconsultingservices.com/smarts.php.)

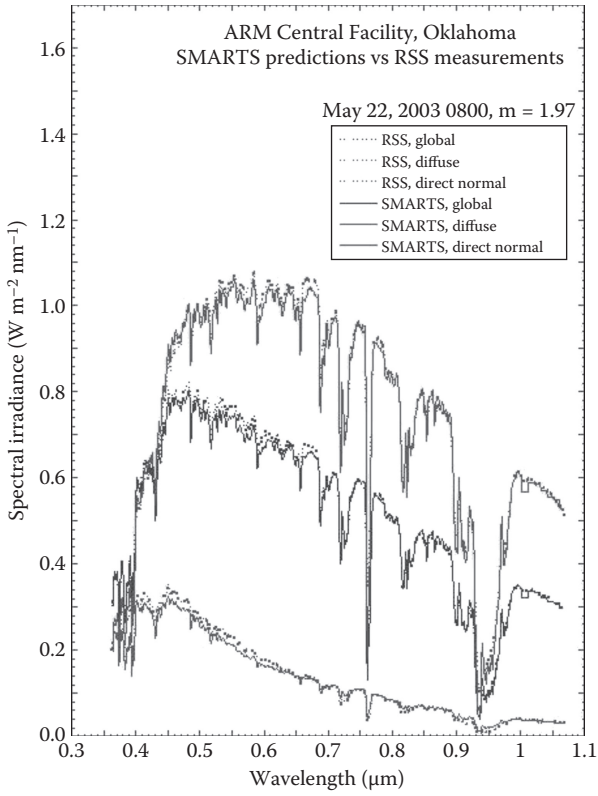

Figure 2.26
A sample prediction for direct normal, diffuse and global horizontal spectral irradiance. (Taken from http://www.solarconsultingservices.com/smarts.php.)

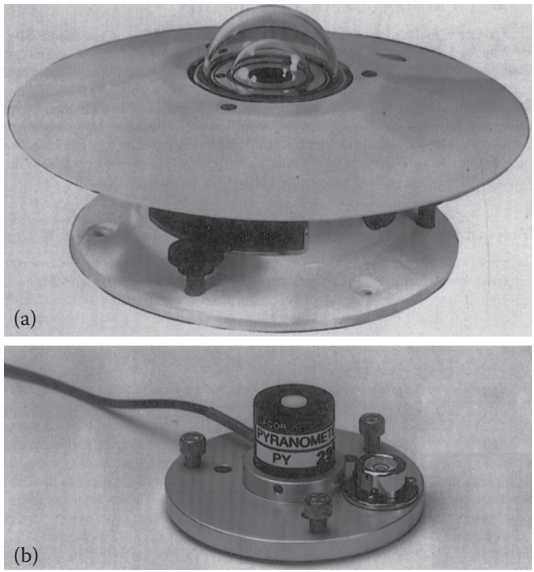

Figure 2.27
Typical commercially available pyranometers with (a) thermal detector and (b) photovoltaic detector.

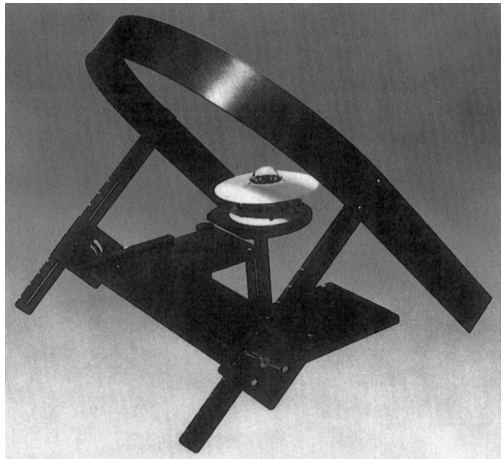

Figure 2.28
A pyranometer with a shade ring to measure sky diffuse radiation.

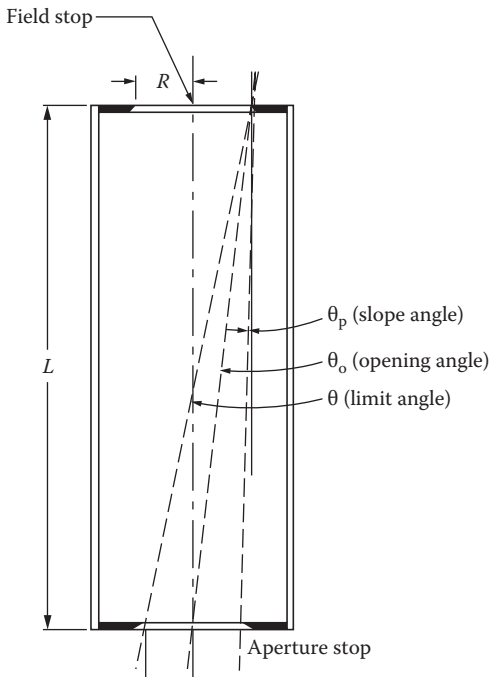

Figure 2.29
Geometry of a pyrheliometer sky occulting tube.

002x029.eps

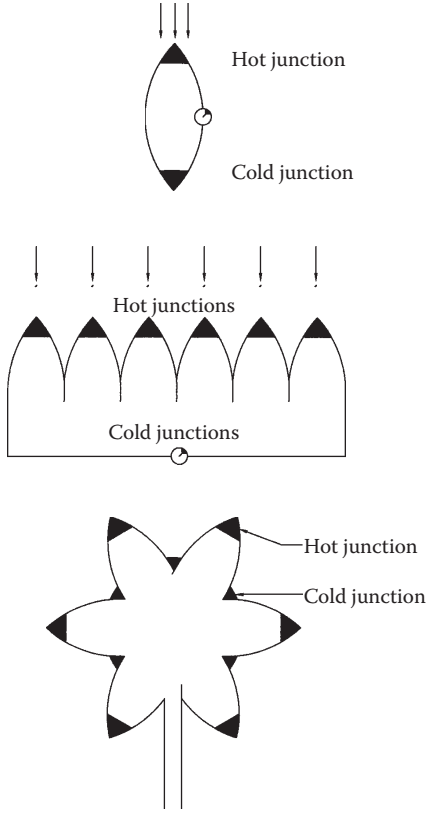

Figure 2.30
Various thermopile configurations. (From Zerlaut, G., Solar radiation instrumentation. In *Solar Resources*, R.L. Hulstrom, ed., Cambridge, MA: MIT Press, 1989.)

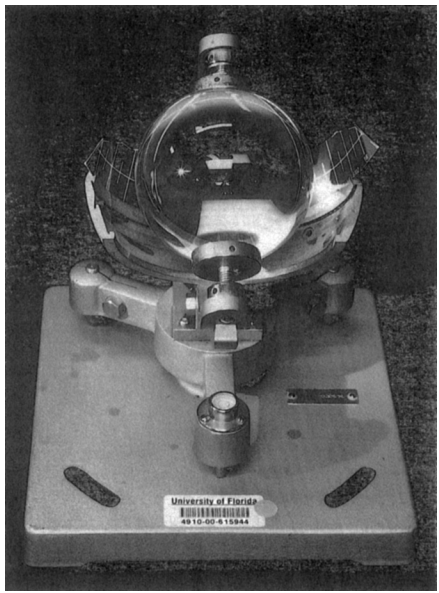

Figure 2.31
Campbell–Stokes sunshine recorder.

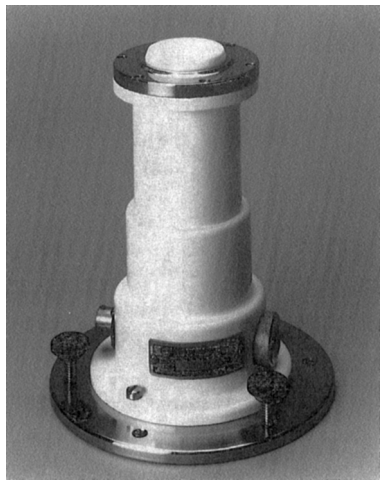

Figure 2.32
Eppley TUVR Total UV Radiometer. (Courtesy of Eppley Lab.)

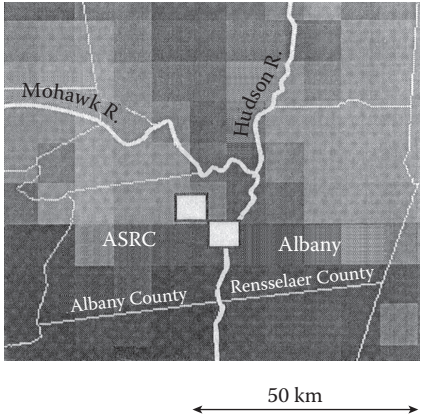

Figure 2.33
GOES-8 Intermediate resolution image close-up around Albany. (From Perez, R. et al., The strengths of satellite based resource assessment. *Proc. of the 1997 ASES Annual Conf*, pp. 303–308, Washington, DC, 1997.)

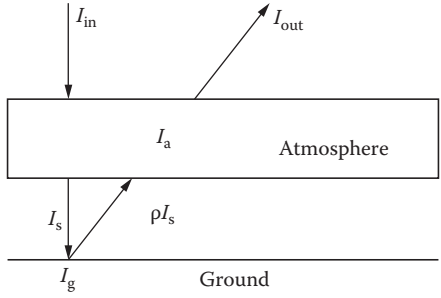

FIGURE 2.34
Solar radiation in the earth-atmosphere model.